Control-oriented Modelling of Vapour-Compression Cycle Including Model-order Reduction and Analysis Tools

Igor Ratković*, Ivan Cvok, Vladimir Soldo, Joško Deur
University of Zagreb, Zagreb, Croatia
Faculty of Mechanical Engineering and Naval Architecture
e–mail: igor.ratkovic@fsb.hr

ABSTRACT

The paper first presents a gradual analytical model-order reduction of a moving boundary method-based 12th-order lumped-parameter nonlinear vapour compression cycle model. Model-order reduction is conducted by introducing certain assumptions and replacing state variables associated with fast dynamics with static expressions. Next, numerical tools implemented in MATLAB/Simulink and applicable to black-box heating, ventilation and air-conditioning (HVAC) models are developed for the purpose of obtaining the model static input-output maps and linearized model parameters for a wide range of operating conditions. The linearized models are used for comparison of pole-zero maps of high- and low-order models, which shows that slower, dominant dynamics are preserved in the reduced-order models. Finally, as an alternative to model-order reduction approach, a multi-input/multi-output model identification approach is proposed, which can provide a low-order linearized model directly from simulated time response of a full-order lumped- or distributed-parameter model, or from real vehicle HVAC test signals.

KEYWORDS

Control-oriented modelling, vapour-compression cycle, HVAC, model order reduction, steady-state analysis, linearization, system identification

INTRODUCTION

An increase in mass market-share of fully electric vehicles (FEV) is hindered by end user's perspective of FEVs having limited driving range compared to conventional vehicles. Besides the electric powertrain system, the heating, ventilation and air-conditioning (HVAC) system has the highest energy consumption and can greatly impact the driving range of the vehicle [1], [2]. This reduction in range can be up to 22% in hot and up to 60% in cold weather [3]. Advanced FEV's HVAC system can work in either air-conditioning (cooling) or heat pump mode (heating), both of which are based on the vapour-compression cycle (VCC). The VCC is a four-stage thermodynamic process which consists of compression, throttling and thermal energy exchange of the circulating working fluid (refrigerant) with an external medium in evaporator and condenser (heat exchangers), during which the working fluid undergoes a phase change. The VCC performance (e.g. in terms of efficiency) is determined by ambient conditions and operating parameters. Optimal control of a HVAC system is crucial for achieving maximum

* Corresponding author

performance under given conditions, thus increasing the driving range. Controller design and optimisation processes require a suitable dynamic model of the plant.

Rasmussen [4], [5] provided an extensive review of different VCC modelling approaches suitable for various applications. For control-oriented modelling purposes, a combination of physics-based models in conjunction with map or data-based models is suggested therein. This provides adequate accuracy and flexibility in terms of providing model use for different operating conditions. Two common approaches for physics-based VCC modelling are finite-volume method and the moving-boundary lumped-parameter method [6], [7]. The finite volume method discretises heat exchanger into arbitrary number of either fixed or variable volumes. Each volume is defined with differential equations which govern its dynamics and boundary conditions. The accuracy of the model and computational load increase with the number of finite volumes. In the moving-boundary method (MBM) each heat exchanger is sub-divided into three specific nodes: superheating, subcooling and the two-phase node. Presence and spatial distribution of individual nodes depend on the operating conditions. Fluids thermophysical properties for each node are calculated by using the lumped parameter approach, averaging the properties as well as heat exchange coefficients over the length of individual phase. Bendapudi et al. [8] have shown that the execution time of finite volume model is three times longer than that of MBM model of similar accuracy. Therefore, the MBM presents a valid compromise between accuracy and numerical complexity which makes it suitable for control-oriented modelling.

This paper presents a 12th-order MBM model. This relatively high-order model is reduced using a step-by-step analytical approach. Each reduction step introduces additional assumptions in order to obtain a control-oriented model. Finally, the developed tools for static input-output model maps generation, model linearization, and system identification are presented. These tools can be readily modified and applicable to black-box models, including the finite-volume ones and the ones describing more complex HVAC system in FEVs (see e.g. [9]). The presented 12th -order model and related tools are used for control trajectory optimisation and optimal control strategy design in [10].

12TH-ORDER VCC MODEL

The VCC model considered in this paper is based on a single-fluid single-stage circuit, R-134a is considered as a working fluid, although any sub-critical cycle refrigerant can be used instead. The configuration of vapour-compression cycle components is shown in Figure 1. A variable-speed fixed-displacement compressor is used for compression, while the throttling of refrigerant is done using an electronic expansion valve (EXV). The refrigerant exchanges thermal energy with an unmixed air-stream in cross-flow heat exchangers through tube wall. Air stream is supplied to evaporator and condenser by a blower fan and an axial fan, respectively. For simplicity, air mass flow rates instead of fan blade speeds are considered as inputs. An extensive list of symbols used in model presentation is given in Nomenclature. The dominant dynamics of the system are tied with the thermal energy exchange of the heat exchangers. Actuator dynamics are faster by an order of magnitude the heat exchanger dynamics and can be modelled as static expressions [11].

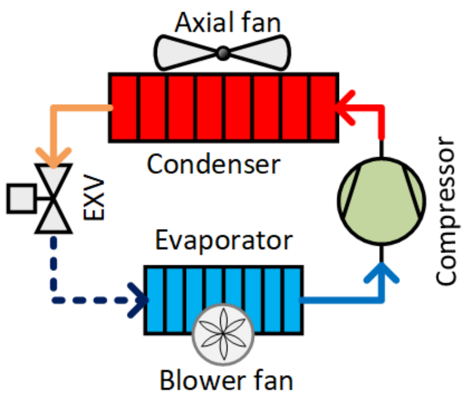

Figure 1: Typical vehicle air-conditioning configuration

Compressor model

Static, efficiency based model of reciprocating compressor with clearance is used for refrigerant mass flow rate calculation [12], [13]:

$$\dot{m}_{com} = \omega_{com} V_{sw} \rho_s \left(1 + C_{com} - C_{com} \left(\frac{p_d}{p_s} \right)^{\frac{1}{n}} \right) \quad (1)$$

It is assumed that the compression process is adiabatic and with constant efficiencies connecting the inlet and outlet enthalpies as given by

$$h_d = \frac{h_{is} - h_s}{\eta_{is}} + h_s \quad (2)$$

Electronic expansion valve model

A simplified expansion valve model is adopted from [11], [14], [15], where the mass flow rate through the valve is defined as:

$$\dot{m}_v = a_v C_v A_v \sqrt{\rho_{co}(p_c - p_e)} \quad (3)$$

where the input value $a_v \in [0,1]$ determines the proportion of valve orifice opening.

Heat exchanger models

Heat exchanger models are based on principles of conservation of mass, energy and momentum for each of the phase-specific nodes [16], [17]. Node boundaries are dynamic variables that determine the spatial distribution of each node within the heat exchanger. Change of operating conditions can cause certain nodes to disappear and/or reappear. For instance, an increase in refrigerant mass flow rate can result in two-phase refrigerant overflowing the heat exchanger, thus eliminating the superheating node. The developed model is suitable only for operating conditions where all nodes are present, since model switching method is not included [18].

Several assumptions and restraints are introduced in order to simplify the complex nature of refrigerant flow and phase change. The working fluid flow is considered frictionless, one-dimensional and the thermal energy exchange between the refrigerant and the wall is considered isobaric. This eliminates the need for momentum conservation equations. The heat exchanger is modelled as a horizontal thin tube with constant cross-section area, with negligible axial and radial heat conduction, resulting in a uniform node wall temperature. Void fraction in the two-phase node that represents the quality of the two-phased mixture is considered time invariant.

On the air-side of the heat exchanger the thermal exchange between the wall and air is considered isobaric and the stream incompressible and at the outlet ideally mixed.

Considering the above assumptions, mass conservation equation can be written as [16]:

$$\frac{\partial \rho}{\partial t} + \frac{\partial \dot{m}}{\partial x} = 0 \tag{6}$$

while the energy conservation equation reads [16]:

$$\frac{\partial(\rho h - p)}{\partial t} + \frac{\delta(\dot{m}h)}{\delta x} = \dot{q} \tag{7}$$

The conservation equations are applied on the working fluid as well as on the tube wall. Integrating Eqs. (6) and (7) from one boundary, e.g. $x = 0$ (inlet), of heat exchanger along the heat exchanger to the beginning of a next phase, e.g. $x = L_1$, is done by using the Leibnitz integration rule which eliminates the spatial dependence of system variables and results in time-dependant differential equations.

$$\int_{x_0}^{L_1(t)} A\frac{\partial \rho}{\partial t}dx + \int_{x_0}^{L_1(t)} \frac{\partial \dot{m}}{\partial x}dx = 0 \tag{8}$$

$$\int_{x_0}^{L_1(t)} A\frac{\partial(\rho h)}{\partial t}dx - \int_{x_0}^{L_1(t)} Ap\,dx + \int_{x_0}^{L_1(t)} \frac{\partial(\dot{m}h)}{\partial x}dx = \int_{x_0}^{L_1(t)} \dot{q}\,dx \tag{9}$$

Thermophysical properties, e.g. density and temperature, are averaged for each node depending on the state of the refrigerant. Phase distribution within each heat exchanger along with their respective state variables and other important parameters for nominal operating conditions is depicted in Figure *2*.

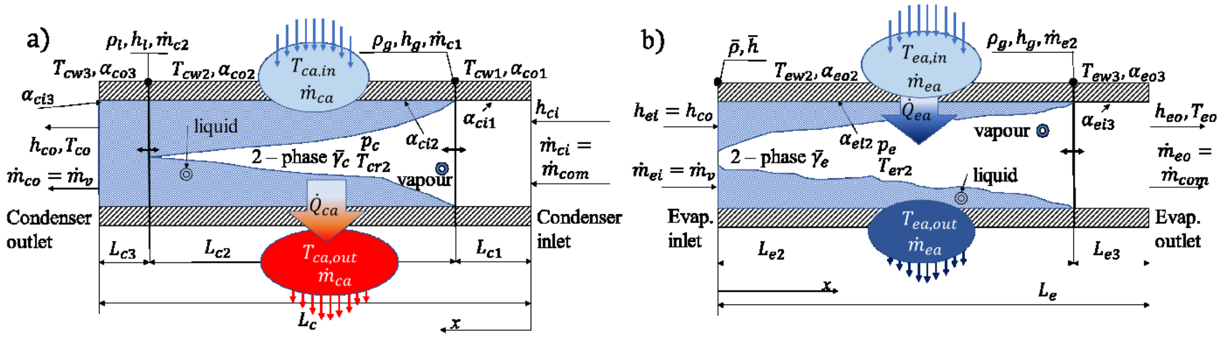

Figure 2: Heat exchanger node specific state variables and parameters

Repeating the integration process for the remaining two nodes and sorting the differential equations to eliminate intermediate mass flows $\dot{m}_1$ and $\dot{m}_2$ between the phases results in a nonlinear 7[th]-order model written in the following matrix form:

$$\mathbf{A}(\mathbf{x})\dot{\mathbf{x}} = \mathbf{f}(\mathbf{x}, \mathbf{u}) \tag{10}$$

where the state variable vector

$$\mathbf{x} = [L_1 \quad L_2 \quad p \quad h_o \quad T_{w1} \quad T_{w2} \quad T_{w3}]^T \tag{11}$$

includes the lengths of first two nodes L_1 and L_2, the refrigerant pressure p, the outlet specific enthalpy h_o, and the node wall temperatures T_{w1}, T_{w2} and T_{w3}. The condenser model contains all three phases, while the evaporator model contains only the two-phase node followed by superheating node. Thus, the evaporator model is obtained by reducing the above model to a

5^{th}-order model (the subcooling node length L_1 and the wall temperature T_{w1} are omitted). The input vector **u**

$$\mathbf{u} = [\omega_{com} \quad a_v \quad \dot{m}_{ea} \quad \dot{m}_{ca}]^T \tag{12}$$

includes the compressor speed ω_{com}, the valve opening a_v, and the air mass flow rate over evaporator ($\dot{m}_{ea}$) and condenser ($\dot{m}_{ca}$).

Overall VCC model

The complete 12^{th} order VCC model is obtained by combining individual model equations, where an output of a model serves as an input to subsequent model and its set of equations (see Figure 3). The model is implemented in the MATLAB/Simulink environment. This enables simulation as well as use of different Matlab-embedded tools for linearization, system identification and control design. CoolProp library [19] is used to obtain fluid properties by interpolating values from fluid-specific nonlinear thermodynamic tables. CoolProp functions require at least two arguments, e.g. pressure and temperature to obtain fluid thermodynamic property.

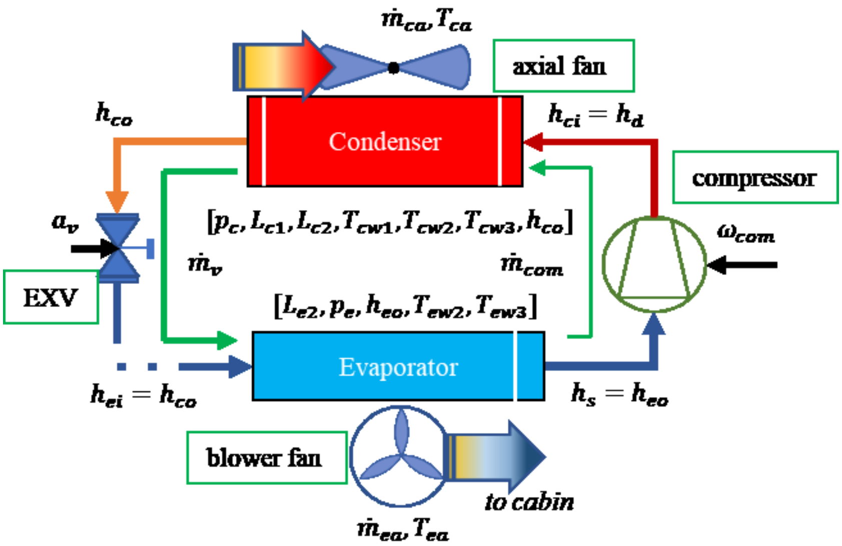

Figure 3: Schematic of the 12th order model of vapour compression cycle with corresponding state variables

Expressions of all elements of the system matrix **A**, as well as the balance equation elements of the vector **f** for the evaporator and the condenser are given in the Appendix A1.

MODEL-ORDER REDUCTION METHOD

The highly nonlinear coupled dynamics of the 12^{th}-order model makes it difficult to assess the effect of individual state variable on overall system dynamics and identify suitable states for reduction. However, it is known that the dominating dynamics of the process is that of thermal energy exchange, while the states associated with mass-transport process have faster dynamics [14]. Therefore, an analytical step-by-step reduction method is applied, gradually eliminating certain state variables. Each sub-sequent reduced model is derived from the higher-order model and inherits the previously introduced assumptions. Overview of all reduced-order models and introduced assumptions is given in Table 1. The reduced-order models have been validated against the full 12^{th}-order model (designated as R12).

Table 1: Overview of model order reduction steps and assumptions

Reduction step / model designation		1 / R9	2 / R8	3 / R6	4 / R5	5 / R3
Leading assumption		Uniform wall temperature	Static superheating node length	Static outlet spec. enthalpy	Static two-phase length	Equal wall and refrigerant temperature
State variables eliminated	Condenser	T_{cw1}, T_{cw2}, $T_{cw3} \rightarrow T_{cw}$	L_{c1}	h_{co}	L_{c2}	T_{cw}
	Evaporator	T_{ew2}, $T_{ew3} \rightarrow T_{ew}$	---	h_{eo}	---	T_{ew}
Final model order		9	8	6	5	3

Uniform heat exchanger wall temperature (R9)

The wall acts as a boundary between the refrigerant and ambient air stream, and the temperature gradient between the wall and those two fluids greatly influences process dynamics. Introducing a uniform wall temperature T_{cw}, which replaces individual node-specific wall temperatures $T_{cw1,2,3}$, reduces the order by two for condenser and one for evaporator resulting in a 9th order (R9) model. The reduction introduces a greater temperature difference between the wall and surrounding fluids, affecting overall thermal energy exchange and phase distribution. However, this can be mitigated by adjusting either (or both) the internal α_i and external α_o heat transfer coefficients to match the heat exchange of the 12th-order model.

Static condenser superheating node length L_{c1} (R8)

In the nominal operating conditions, most of the thermal energy exchange occurs in the two-phase node. Therefore, the two-phase node L_{c2} dictates the dynamics while the length of the superheating node L_{c1} has minor effect on the overall condenser. Boundary conditions of the first node are defined by the remaining state variables p_c and T_{cw1} and its inlet h_{ci} and outlet h_{cg} enthalpies, enabling the replacement of the state-variable dynamics with a static expression:

$$L_{c1} = \frac{\dot{m}_{ci}\left(h_{ci} - h_{cg}\right)}{\alpha_{ci1} D_{ci} \pi (\bar{T}_{r1} - T_{cw})} \tag{13}$$

This reduces the model order to 8th order (R8).

Static heat exchanger outlet specific enthalpy (R6)

Specific enthalpy at the outlet h_{ko} is a boundary condition that is a result of the slower, thermal energy exchange done in the heat exchanger and as such can be presumed static. The temperature at the heat exchanger outlet T_{ko} (from which the specific enthalpy can be obtained), can be determined by calculating the energy exchange between the refrigerant and the wall on the third node length L_{k3} (defined by other two nodes).

$$T_{ko} = \frac{2\alpha_{ki3} A_{ki} (L_k - L_{k2}) T_{kw} + T_{kr2} \left(2 c_{p,kr} \dot{m}_{kr} - \alpha_{ki3} A_{ki} (L_k - L_{k2})\right)}{2 c_{kp,r} \dot{m}_{kr} + \alpha_{ki3} A_{ki} (L_k - L_{k2})} \tag{14}$$

$$h_{ko} = f(p_k, T_{ko}) \tag{15}$$

The specific enthalpy at the outlet is h_{ko} used to calculate the refrigerant density ρ_{ko} which in turn is used to determine the refrigerant mass flow rates (Eqs. (1) and (3)), thus forming an algebraic loop. This imposes a limitation on the reduced, 6th order model (R6), as a nonlinear dynamic model becomes viable only with the use of a memory block. Figure 4shows the response of R12 and R6 (with memory blocks) to a step change in compressor and valve inputs (Figure 4e and f). The dominant, slow heat exchanger pressure dynamics (Figure 4a and b) are preserved after two steps of reduction. The difference in the evaporator outlet air $T_{ea,out}$ dynamics (Figure 4c) is caused by the uniform wall temperature T_{ew} introduced in R9.

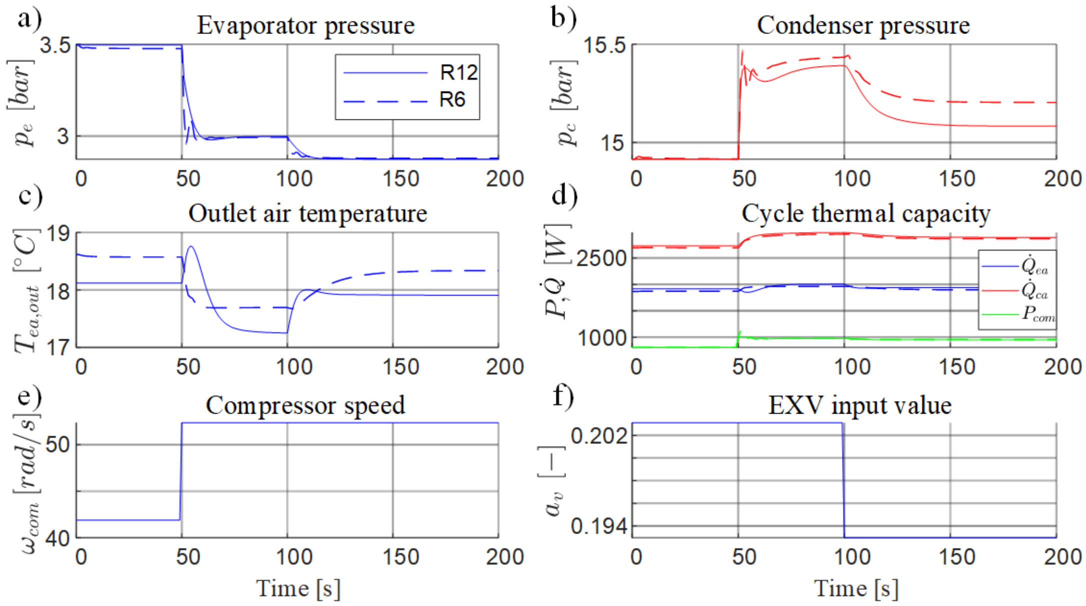

Figure 4: Response of nonlinear R12 and R6 (with memory blocks) models to a step change in compressor and EXV input

R6 system evaporator matrix $\mathbf{A}_{e,R6}$ and condenser matrix $\mathbf{A}_{c,R6}$ with the respective balance equation vector $\mathbf{f}_{e,R6}$ and $\mathbf{f}_{c,R6}$ are given in the appendix A2.

Static condenser two-phase node length (R5)

Since phase-distribution within the condenser is not considered to be of primary concern in controller design, the length of two-phase node within the condenser, L_{c2}, can be replaced with a static expression. The boundary conditions of the two-phase node are defined by pressure p_c and the length of the two-phase can be calculate from the thermal balance equation for the node.

$$L_{c2} = \frac{\dot{m}_{ci} h_{cg} - \dot{m}_{co} h_{cl}}{\alpha_{ci2} A_{ci} (T_{cr2} - T_{cw})} \tag{16}$$

This reduces the model to a 5th-order (R5) which retains the node phase distribution within the condenser.

FURTHER REDUCTION STEPS (R3)

Zhang et al. [20] presented a second order lumped-parameter VCC model, with system pressures p_e and p_c as only state variables. The elimination of wall temperature dynamics was based on the assumptions that in nominal operating conditions the wall temperature is almost equal to the temperature of the two-phase section. The thermal wall inertia was lumped into refrigerant thermal mass and the rate of wall temperature change was assumed to be equal to the time rate of change of saturation temperature at refrigerant pressure. This connects the wall dynamics indirectly to pressure dynamics. Temperature at the evaporator outlet T_{eo} is set to have constant superheat temperature difference ΔT_{SH} = 5 °C for all operating points making the 2nd -order model unsuitable for control design, since it lacks the control input for EXV.

Introducing the assumption of equal wall and refrigerant temperature from second-order model to R5 model would result in a 3rd -order model (R3). Thus, the R3 would describe heat exchanger pressure dynamics, p_e and p_c, and additional evaporator two-phase length dynamics, L_{e2}. In this way, the R3 model would keep the expansion valve opening input and superheat temperature output, which are eliminated in second-order model. Due to the thermal mass lumping, the thermal energy exchange would bypass wall, i.e. it would occur between refrigerant and air requiring the use of an effectiveness-number of transfer units (ε-NTU) method to calculate heat exchange for each node [21].

MODLE STATIC MAPPING, LINEARIZATION AND IDENTIFICATION

Static input-output maps

HVAC system static maps provide a useful tool for analysis of steady-state input-output relationships that can provide insight into HVAC system behaviour. These maps can also serve for the purpose of qualitative model validation in terms of checking if expected trends appear (e.g. evaporator outlet air temperature drop for increased compressor speed). Furthermore, state-variable static maps can facilitate model linearization in terms of providing input, output and state variable steady-state operating point, without need for use cumbersome trim routines. Finally, static maps can conveniently be used in in cabin thermal comfort control trajectory optimisation and feedback controller design, where it is assumed that HVAC dynamics are faster than cabin air temperature dynamics [10].

An automated numerical mapping procedure/tool has been developed based on repetitive running of simulation model. The procedure consists of initializing the model in an a priori known steady-state condition and slowly ramping one of the inputs from the initial value to the end value at a prescribed rate. Once the end value is reached, all inputs are held constant for certain time to allow the system to reach steady state. The obtained steady-state output and input values (and state variables if needed) are stored in m-dimensional matrix where m is the number of varied inputs (e.g. a 3D matrix for the case of three inputs), while the number of outputs defines the number of produced maps. The procedure is repeated for all values of the first input, and then again for different combination of other inputs. Increase in number of inputs and/or input resolution results in prolonged procedure run-time, so that these parameters should be carefully set depending on target application. Additionally, final maps can be filtered with respect to certain input and/or output thresholds and additional criteria in order to obtain smaller maps. For example, the map in Figure 5a is obtained by imposing the desired superheat temperature (ΔT_{SHd} = 15 °C for $\dot{m}_{ea}$ = 0.02 kg/s and ΔT_{SHd} = 5 °C for $\dot{m}_{ea}$ = 0.075 kg/s and above), for each air mass flow rate input combination (to eliminate the expansion valve opening as an input) and minimum evaporator air outlet temperature ($T_{ea,out}$ = 273 K), and then extracting the subset of operating points from the final map whose superheat temperature is closest to the desired value and evaporator air outlet temperature is greater than the prescribed minimum. This procedure is applicable to white-, grey-, and black-box models.

Figure 5 shows two map examples obtained in MATLAB/Simulink for the 12th order HVAC model. Figure 5a shows evaporator outlet air temperature map as a function of three inputs (compressor speed, and two air mass flow rates) for a fixed ambient air temperature and the aforementioned superheat temperature. The map indicates that for a fixed evaporator air mass flow rate $\dot{m}_{ea}$, the evaporator outlet air temperature $T_{ea,out}$ drops with increased compressor speed ω_{com}, while for fixed ω_{com}, the air temperature $T_{ea,out}$ increases with increased $\dot{m}_{ea}$. This suggests that higher evaporator cooling power is needed to lower the air temperature at increased air mass flow rates. For the particular HVAC parameters, at highest evaporator air mass flow rate $\dot{m}_{ea}$ = 0.13 kg/s the air cannot be cooled lower than $T_{ea,out}$ = 15 °C for maximum condenser air mass flow rate. The condenser air mass flow rate $\dot{m}_{ca}$ has a low influence on the evaporator air outlet temperature ($T_{ea,out}$ slightly decreases by increasing $\dot{m}_{ca}$). Figure 5b shows the evaporator outlet air temperature and the superheat temperature as a function of compressor speed and expansion valve opening for fixed ambient air temperature and air mass flow rates. It indicates that in order to keep the superheat temperature in desired range while decreasing the evaporator air outlet temperature, the expansion valve opening should increase with compressor speed.

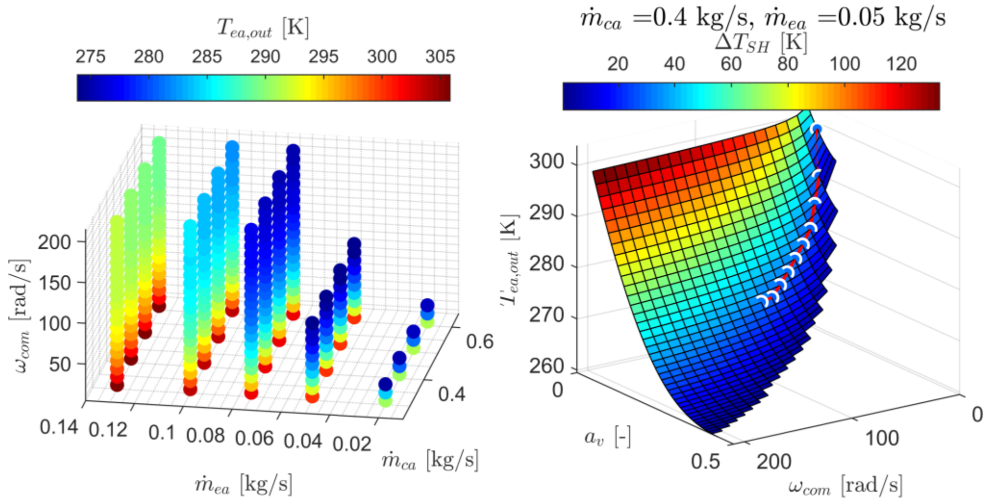

Figure 5: Filtered evaporator outlet air temperature map for fixed superheat temperatures (ΔT_{SHd} = 15 °C for $\dot{m}_{ea}$ = 0.02 kg/s and ΔT_{SHd} = 5 °C for $\dot{m}_{ea}$ = 0.075 kg/s and above) (a) and evaporator outlet air temperature and superheat temperature map for fixed air mass flow rates where red line corresponds to corresponding column in Fig. a (b).

Linearization

Numerical linearization tool has been developed within the MATLAB/Simulink environment. The tool takes a nonlinear model of the system, finds the operating points (using function *findop*) for specified inputs and desired outputs, or loads the operating point stored in static maps, and linearizes the model around the trimmed operating point. This operation is indifferent to the model order and can be applied to black-box models (created or imported into Simulink), as well. Inputs that are not considered as control variables, such as those stored in memory blocks, are replaced by constant-value operating point-dependent inputs. Linearization results in a linear time-invariant state-space model suitable for further linear analysis and controller design. The obtained linearized models can serve in validation of reduced-order models based on step response or pole-zero map comparisons. Figure 6 shows the comparative step response of full-order R12 model and the reduced-order R6 model, both given in nonlinear and linearized variants. The difference in inital outlet evaporator air temperature $T_{ea,out}$ between R12 and R6 is due to different initial wall temperatures. Namely, the single wall temperature T_{ew} introduced in R9 (and kept in R6) slows down the overall dynamics of evaporator heat exchange due to lesser temperature gradient between the wall and individual nodes. This difference can be mitigated by adjusting the internal and external heat transfer coefficients. Pressure dynamics for both evaporator and condenser are well preserved in the reduced-order model. Expectedly, the linearized models give responses that are close to the original, nonlinear models for the considered small-signal operating mode (for which a linearized model is valid/obtained).

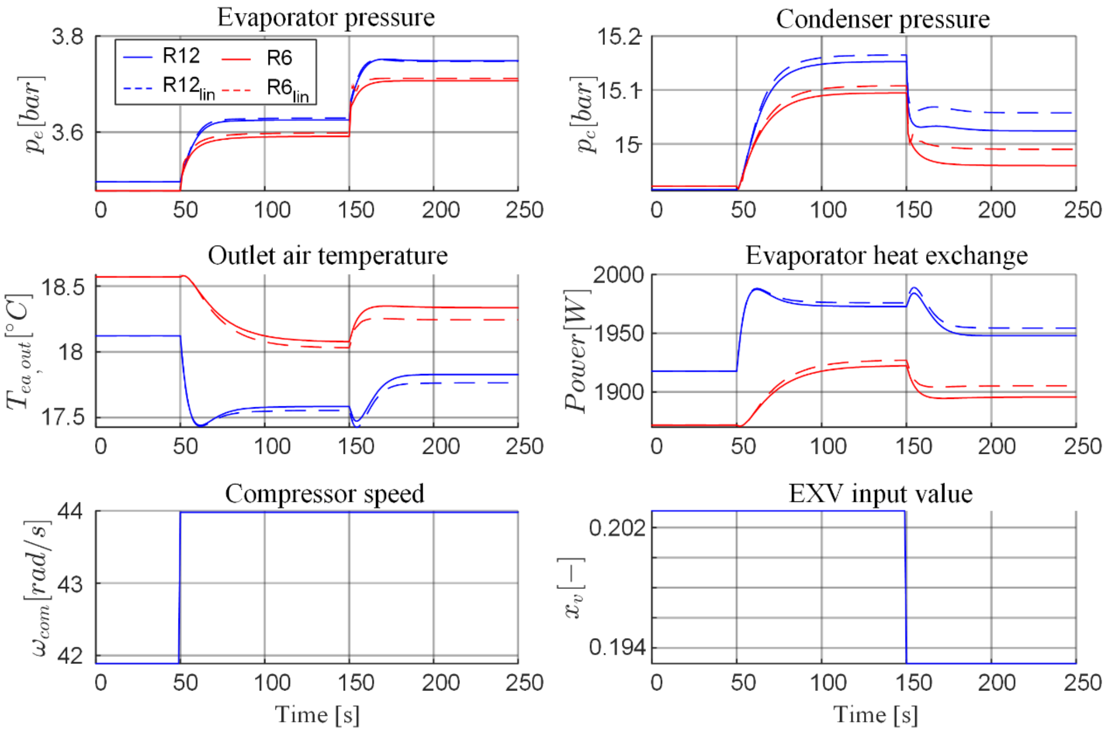

Figure 6: Response of nonlinear and linearized R12 model to a step change in compressor speed and EXV opening

Model identification

Low-order control-oriented linear models can alternatively be obtained by applying model identification methods, either based on high-order nonlinear models or real system experimental responses. Model identification bypasses the need for model-order reduction and is easily applicable to black-box HVAC models of any structure, which makes it particularly interesting for HVAC control design purposes, particularly for cooperative projects (such as QUIET), where a partner develops the model and delivers it to another partner for designing controls.

A numerical tool for obtaining multi-input multi-output autoregressive exogenous (ARX)-type HVAC model has been developed in MATLAB. For the purposes of HVAC low-level control design, identification of a two-input/two-output discrete-time ARX model is considered, with the the model having following structure:

$$\begin{aligned}
&\mathbf{A}_{11}(z)y_1(k) = -\mathbf{A}_{12}(z)y_2(k) + \mathbf{B}_{11}(z)u_1(k-n_{k11}) + \mathbf{B}_{12}(z)u_2(k-n_{k12}) + \mathbf{e}_1(k) \\
&\mathbf{A}_{22}(z)y_2(k) = -\mathbf{A}_{21}(z)y_1(k) + \mathbf{B}_{11}(z)u_1(k-n_{k21}) + \mathbf{B}_{12}(z)u_2(k-n_{k22}) + \mathbf{e}_2(k) \\
&\mathbf{A}_{ij}(z) = 1 + a_{ij,1}z^{-1} + \ldots \qquad z^{-n_{ij,a}}, \qquad i = 1,2, \qquad j = 1,2 \\
&\mathbf{B}_{ij}(z) = b_{ij,1} + b_{ij,2}z^{-1} + \ldots \qquad z^{-n_{ij,b}+1}
\end{aligned} \tag{17}$$

where $u_1 = \omega_{com}$, $u_2 = a_v$, $y_1 = T_{ea,out}$, $y_2 = \Delta T_{SH}$, $n_{ij,a}$ is the order of polynomial $\mathbf{A}_{ij}(z)$, $n_{ij,b}$ is the order of polynomial $\mathbf{B}_{ij}(z)$+1, and n_k is the input-output delay and z is the time-shift operator. The order of each polynomial is set separately in advance, and the sum of orders determines the number of coefficients to be determined by setting a linear regression problem and using a least-squares method. Model identification procedure is implemented in MATLAB by using System Identification Toolbox *arx* function. Multiple models with various polynomial orders can be identified in a automated way, and assessed taking into account fitness and complexity in order to obtain optimal model structure.

ARX model identification is demonstrated for a single operating point of the 12th-order model, where the evaporator outlet air temperature and the superheat temperature are outputs and the compressor speed and the expansion valve opening are inputs. Simulation data set contains multiple step-responses around the initial operating point: $T_{ea,out}$ = 8 °C, ΔT_{SH} = 8 °C, ω_{com} = 80 rad/s, a_v = 0.3, $\dot{m}_{ca}$ = 0.5 kg/s and $\dot{m}_{ea}$ = 0.075 kg/s. The simulation data are sampled at 0.1 s. Two models are considered: ARX1 with all $\mathbf{A}_{ij}$ and $\mathbf{B}_{ij}$ polynomial orders set to three, and ARX2 with polynomial orders set to six, while input-output delay is set to zero in both cases. Figure 7 a-d show data set used in model identification based on simulation of R12 model (black lines) and time responses of identified models. The higher-order model (blue line) results in lower normalized root-mean squared error (i.e. higher fitness index denoted in label) than the lower-order model (red line) and matches the transient response of simulated data to better extent, while both models satisfy steady-state accuracy**.** Figure 7 e-h show validation data set (black lines) and time responses of identified models. The results indicate that slight steady-state discrepancy occurs between linear ARX model time responses and simulation data for the case of increased magnitude of inputs, while the transient response is well matched.

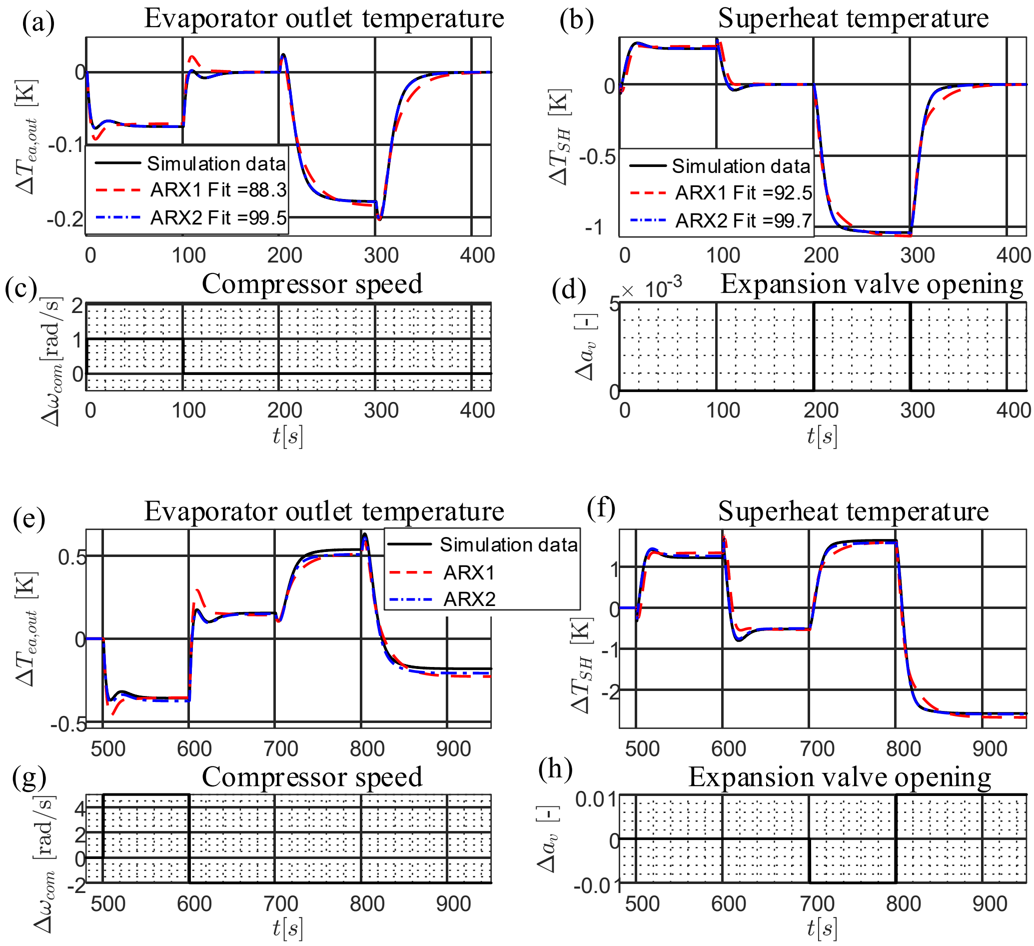

Figure 7: Model identification input data (black lines) and time responses of ARX1 model with third-order polynomials (red line) and ARX2 model with sixth-order polynomials (blue line) for identification data set (a-d) and validation data set (e-h)

CONCLUSION *

A 12th-order moving-boundary mathematical model of a vapor-compression cycle has been presented and implemented in MATLAB/Simulink having in mind electric vehicle HVAC control applications. An analytical model order reduction based on introducing additional assumptions has been carried out and resulted in several lower-order models. The reduction process ends with a third-order model, which describes condenser and evaporator pressure dynamics and the evaporator two-phase node length dynamics.

A numerical tool for input/output model static mapping has been developed, which results in multiple, multi-dimensional maps describing system steady-state behaviour. Static maps can be used in system analyses, model linearization and computationally-efficient control trajectory optimisation for cabin thermal comfort. The numerical tool has been extended to provide linearized model around an arbitrary static operating point. Finally, a model identification procedure has been developed as an alternative to model-order reduction method. This procedure gives a representative low-order multi-input/multi-output linear model directly from a nonlinear model of any type (e.g. white or black box one, lumped- or distributed-parameter one). The numerical tools have been successfully validated based on the 12th-order nonlinear HVAC model, and further used in control system design and optimisation study in [10].

ACKNOWLEDGEMENT

It is gratefully acknowledged that this work has been supported through QUIET project (Qualifying and implementing a user-centric designed and efficient electric vehicle), which has received funding from the European Union’s Horizon 2020 Research and Innovation Programme under Grant agreement No. 769826. In addition, the research work of the second author has been partly supported by the Croatian Science Foundation through the "Young researchers’ career development project – training of new doctoral students".

NOMENCLATURE

A	$[m^2]$	cross-section area	h	$[J/kg]$	specific enthalpy	$\dot{Q}$	$[W]$	heat flow
$\mathbf{A}$	$[-]$	system matrix	L	$[m]$	length	t	$[s]$	time
a_v	$[-]$	valve control input	m	$[kg]$	mass	T	$[K]$	temperature
c_p	$\left[\frac{J}{kgK}\right]$	specific heat capacity at const. press.	$\dot{m}$	$\left[\frac{kg}{s}\right]$	mass flow rate	$\mathbf{u}$	$[-]$	input vector
C_v	$[-]$	orifice hydraulic coefficient	n	$[-]$	polytropic coefficient or pump speed	V	$[m^3]$	volume
C	$[-]$	clearance factor	P	$[W]$	power	x	$[m]$	position
D	$[m]$	diameter	p	$[Pa]$	pressure	$\mathbf{x}$	$[-]$	state vector
$\mathbf{f}$	$[-]$	conservation matrix	$\dot{q}$	$\left[\frac{W}{kg}\right]$	specific heat flow	$\bar{x}$	$[-]$	averaged value of x

Greek symbols					
α	$\left[\frac{W}{m^2K}\right]$	heat transfer coefficient	η	$[-]$	efficiency
γ	$[-]$	void fraction	ρ	$\left[\frac{kg}{m^3}\right]$	fluid density

ε	$[-]$	heat exchanger effectiveness factor	ω	$[rad/s]$	compressor speed

Subscripts

a	air or ambient	l	liquid phase
c	condenser or clearance (compressor)	o	outlet or outer
com	compressor	r	refrigerant
e	evaporator	SH	superheat temperature
g	vapour (gas) phase	sw	swept
i	inlet or inner	v	valve / orifice
is	isentropic	w	tube wall
k	denotes condenser or evaporator		

REFERENCES

[1] J. Pouladi, M. B. Bannae Sharifian, and S. Soleymani, "Determining charging load of PHEVs considering HVAC system and analyzing its probabilistic impacts on residential distribution network," *Electr. Power Syst. Res.*, vol. 141, pp. 300–312, Dec. 2016.

[2] K. Vatanparvar and M. A. Al Faruque, "Battery lifetime-aware automotive climate control for electric vehicles," in *Proceedings of the 52nd Annual Design Automation Conference on - DAC '15*, 2015, pp. 1–6.

[3] E. Paffumi *et al.*, "Experimental Test Campaign on a Battery Electric Vehicle: On-Road Test Results (Part 2)," *SAE Int. J. Altern. Powertrains*, vol. 4, no. 2, pp. 2015-01–1166, Apr. 2015.

[4] B. D. Rasmussen and A. Jakobsen, "Review of compressor models and performance characterizing variables.," in *International Compressor Engineering Conference*, 2000, pp. 515–522.

[5] B. P. Rasmussen and B. Shenoy, "Dynamic modeling for vapor compression systems-Part II: Simulation tutorial," *HVAC R Res.*, vol. 18, no. 5, pp. 956–973, 2012.

[6] H. Pangborn, A. G. Alleyne, and N. Wu, "A comparison between finite volume and switched moving boundary approaches for dynamic vapor compression system modeling," *Int. J. Refrig.*, vol. 53, pp. 101–114, May 2015.

[7] H. Qiao, R. Radermacher, and V. Aute, "A review for numerical simulation of vapor compression systems," in *International Refrigeration and Air Conditioning Conference*, 2010.

[8] S. Bendapudi, J. E. Braun, and E. A. Groll, "A comparison of moving-boundary and finite-volume formulations for transients in centrifugal chillers," *Int. J. Refrig.*, vol. 31, no. 8, pp. 1437–1452, Dec. 2008.

[9] P. Drage, M. Hinteregger, G. Zotter, and M. Šimek, "Cabin Conditioning for Electric Vehicles," *ATZ Worldw.*, vol. 121, no. 2, pp. 44–49, Feb. 2019.

[10] I. Cvok, B. Škugor, and J. Deur, "Control Trajectory Optimisation and Optimised Control of Electric Vehicle HVAC System for Favourable Thermal Comfort," in *14th SDEWES Conference*, 2019.

[11] B. P. Rasmussen and A. G. Alleyne, "Control-oriented modeling of transcritical vapor compression systems," *J. Dyn. Syst. Meas. Control. Trans. ASME*, vol. 126, no. 1, pp. 54–64, 2004.

[12] J. Jabardo, W. Mamani, and M. R. Ianella, "Modeling experimental evaluation of an automotive air conditioning system with a variable capacity compressor," *Int. J. Refrig.*, vol. 25, no. 8, pp. 1157–1172, 2002.

[13] Q. Zhang, "Modeling , Energy Optimization and Control of Vapor Compression Refrigeration Systems for Automotive Applications," 2014.

[14] X.-D. He, S. Liu, H. H. Asada, and H. Itoh, "Multivariable control of vapor compression systems," *HVAC R Res.*, vol. 4, no. 3, pp. 205–230, 1998.

[15] H. Li, J. E. Braun, and B. Shen, "Modeling Adjustable Throat-Area Expansion Valves," *Int. Refrig. Air Cond. Conf.*, no. 1, pp. 1–10, 2004.

[16] E. W. Grald and J. W. MacArthur, "A moving-boundary formulation for modeling

time-dependent two-phase flows," *Int. J. Heat Fluid Flow*, vol. 13, no. 3, pp. 266–272, 1992.

[17] B. D. Eldredge, B. P. Rasmussen, and A. G. Alleyne, "Moving-Boundary Heat Exchanger Models With Variable Outlet Phase," *J. Dyn. Syst. Meas. Control*, vol. 130, no. 6, p. 061003, 2008.

[18] J. Bonilla, L. J. Yebra, S. Dormido, and E. Cellier, "Object-Oriented Modeling of Switching Moving Boundary Models for Two-phase Flow Evaporators," *Mathmod*, 2012.

[19] I. H. Bell, J. Wronski, S. Quoilin, and V. Lemort, "Pure and Pseudo-pure Fluid Thermophysical Property Evaluation and the Open-Source Thermophysical Property Library CoolProp," *Ind. Eng. Chem. Res.*, vol. 53, no. 6, pp. 2498–2508, Feb. 2014.

[20] Q. Zhang and M. Canova, "Lumped-parameter modeling of an automotive air conditioning system for energy optimization and management," *ASME 2013 Dyn. Syst. Control Conf. DSCC 2013*, vol. 1, 2013.

[21] H. A. Navarro, L. Cabezas-Gómez, J. R. B. Zoghbi Filho, G. Ribatski, and J. M. Saiz-Jabardo, "Effectiveness - NTU data and analysis for air conditioning and refrigeration air coils," *J. Brazilian Soc. Mech. Sci. Eng.*, vol. 32, no. 3, pp. 218–226, Sep. 2010.

APPENDIX

A1. 12th order model

Condenser model is defined with the system matrix $\mathbf{A}_c$

$$\mathbf{A}_c = \begin{bmatrix} A_c\bar{\rho}_1(\bar{h}_1 - h_1) & A_cL_{c1}\left(\frac{d(\bar{\rho}_1\bar{h}_1)}{dp_c} - \frac{d\bar{\rho}_1}{dp_c}h_1\right) & 0 & 0 & 0 & 0 & 0 \\ A_c\bar{\rho}_3(h_2 - \bar{h}_3) & A_cL_{c3}\left(\frac{d(\bar{\rho}_3\bar{h}_3)}{dp_c} - \frac{d\bar{\rho}_3}{dp_c}h_2\right) & A_c\bar{\rho}_3(h_2 - \bar{h}_3) & \frac{1}{2}A_cL_{c3}\left(\bar{\rho}_3 + \frac{d\rho_3}{dh}|_{p_c}(\bar{h}_3 - h_2)\right) & 0 & 0 & 0 \\ A_c(\bar{\rho}_1 - \bar{\rho}_3) & A_cL_{c2}\left(\frac{d\rho_{lg}}{dp_c} + \frac{d\bar{\rho}_1}{dp_c} + \frac{d\bar{\rho}_3}{dp_c}\right) & A_c(\rho_{lg} - \bar{\rho}_3) & \frac{1}{2}A_cL_{c3}\frac{d\rho_3}{dh}|_{p_c} & 0 & 0 & 0 \\ A_c(\bar{\rho}_1h_1 - \bar{\rho}_3h_2) & A_c\left(L_{c2}\left(\frac{d(\rho h)_{lg}}{dp_c} - 1\right) + L_{c1}\frac{d\bar{\rho}_1}{dp_c}h_1 + L_{c3}\frac{d\bar{\rho}_3}{dp_c}h_2\right) & A_c((\rho h)_{lg} - \bar{\rho}_3h_2) & \frac{1}{2}A_cL_{c3}\frac{d\rho_3}{dh}|_{p_c}h_2 & 0 & 0 & 0 \\ -(T_{cw2} - T_{cw1}) & 0 & 0 & 0 & L_{c1} & 0 & 0 \\ (T_{cw2} - T_{cw3}) & 0 & -(T_{cw3} - T_{cw2}) & 0 & 0 & L_{c2} & 0 \\ (T_{cw3} - T_{cw3}) & 0 & (T_{cw3} - T_{cw3}) & 0 & 0 & 0 & L_{c3} \end{bmatrix}$$

and with conservation balance vector $\mathbf{f}_c$ that contains mass balance and heat exchange elements for the overall length of the condenser L_c

$$\mathbf{f}_c = \begin{bmatrix} \dot{m}_{ci}(h_{ci} - h_1) - \dot{Q}_{cr1} \\ -\dot{Q}_{cr3} - \dot{m}_{co}(h_{co} - h_2) \\ \dot{m}_{ci} - \dot{m}_{co} \\ -\dot{Q}_{cr2} + \dot{m}_{ci}h_1 - \dot{m}_{co}h_2 \\ \frac{\dot{Q}_{cr1} - \dot{Q}_{ca1}}{(c_pm/L_c)_w} \\ \frac{\dot{Q}_{cr2} - \dot{Q}_{ca2}}{(c_pm/L_c)_w} \\ \frac{\dot{Q}_{cr3} - \dot{Q}_{ca3}}{(c_pm/L_c)_w} \end{bmatrix}$$

where the thermal energy exchange between the refrigerant and heat exchanger wall for *j*-th node is given by

$$\dot{Q}_{krj} = \dot{m}_{kij}h_{kij} - \dot{m}_{koj}h_{koj} = \pm\,\alpha_{kij}A_{kij}(\bar{T}_{krj} - T_{kwj}) \tag{13}$$

while the thermal exchange between the wall and ambient air is calculated as

$$\dot{Q}_{kaj} = c_{p,a}\dot{m}_{ka}(T_{ka,in} - \bar{T}_{ka,out}) = \pm\,\alpha_{ko}A_{ko}(\bar{T}_{ka} - T_{kw}) \tag{14}$$

where the subscript *k* refers to either condenser or evaporator.

Evaporator model is defined with the system matrix $\mathbf{A}_e$

$$\mathbf{A}_e = \begin{bmatrix} A_eL_{e3}\left(\frac{d(\bar{\rho}_{e3}\bar{h}_{e3})}{dp_e} - \frac{d\bar{\rho}_{e3}}{dp_e}h_{e2}\right) & A_e\bar{\rho}_{e3}(h_{e2} - \bar{h}_{e3}) & \frac{1}{2}A_eL_{e3}\left(\bar{\rho}_{e3} + \frac{d\rho_{e3}}{dh}|_{p_e}(\bar{h}_{e3} - h_{e2})\right) & 0 & 0 \\ A_e\left(L_{e2}\frac{d\rho_{elg}}{dp_e} + L_{e3}\frac{d\bar{\rho}_{e3}}{dp_e}\right) & A_e(\rho_{elg} - \bar{\rho}_3) & \frac{1}{2}A_eL_{e3}\frac{d\rho_{e3}}{dh}|_{p_e} & 0 & 0 \\ A_e\left(L_{e2}\left(\frac{d(\rho h)_{elg}}{dp_e} - 1\right) + L_{e3}\frac{d\bar{\rho}_3}{dp_3}h_{e3}\right) & A_e((\rho h)_{elg} - \bar{\rho}_3h_{e2}) & \frac{1}{2}A_eL_{e3}\frac{d\rho_{e3}}{dh}|_{p_e}h_2 & 0 & 0 \\ 0 & -(T_{ew3} - T_{ew2}) & 0 & L_{e2} & 0 \\ 0 & (T_{ew2} - T_{ew3}) & 0 & 0 & L_{e3} \end{bmatrix}$$

and with the conservation balance vector $\mathbf{f}_e$ that contains mass balance and heat exchange elements for the overall length of the evaporator L_e

$$\mathbf{f}_e = \begin{bmatrix} \dot{Q}_{er3} - \dot{m}_{eo}(h_{eo} - h_{e2}) \\ \dot{m}_{ei} - \dot{m}_{eo} \\ \dot{Q}_{er2} + \dot{m}_{ei}h_{ei} - \dot{m}_{eo}h_{e2} \\ \dfrac{\dot{Q}_{ea2} - \dot{Q}_{er2}}{\left(c_p m/L_e\right)_{ew}} \\ \dfrac{\dot{Q}_{ea3} - \dot{Q}_{er3}}{\left(c_p m/L_e\right)_{ew}} \end{bmatrix}$$

A2. 6th order model

The outlet specific enthalpies h_{eo} and h_{co}, i.e. the corresponding temperatures T_{eo} and T_{co} are assumed to be determined through static relations, given by:

$$T_{eo} = \frac{2\alpha_{ei3}A_{ei}(L_e - L_{e2})T_{ew} + T_{er2}\left(2c_{p,r}\dot{m}_{com} - \alpha_{ei3}A_{ei}(L_e - L_{e2})\right)}{2c_{p,r}\dot{m}_{com} + \alpha_{ei3}A_{ei}(L_e - L_{e2})}$$

Condenser outlet temperature T_{co} is calculated:

$$T_{co} = \frac{2\alpha_{crw3}D_{ci}\pi(L_c - L_{c2} - L_{c1})T_{cw} + T_{cr2}\left(2c_{p,r}\dot{m}_v - \alpha_{crw3}D_{ci}\pi(L_c - L_{c2} - L_{c1})\right)}{2c_{p,r}\dot{m}_v + \alpha_{crw3}D_{ci}\pi(L_c - L_{c2} - L_{c1})}$$

Reduced condenser state vector now has the following form:

$$\boldsymbol{x}_{c,R6} = [p_c \quad L_{c2} \quad T_{cw}]^T$$

Reduced R8 condenser matrix $\mathbf{A}_{c,R6}$ now has the following form:

$$\mathbf{A}_{c,R6} = \begin{bmatrix} A_c\left(\dfrac{d\rho_{lg}}{dp_c} + \dfrac{d\bar{\rho}_1}{dp_c} + \dfrac{d\bar{\rho}_3}{dp_c}\right) & A_c\left(\rho_{lg} - \bar{\rho}_3\right) & 0 \\ A_c\left(L_{c2}\left(\dfrac{d(\rho h)_{lg}}{dp_C} - 1\right) + L_{c1}\dfrac{d\bar{\rho}_1}{dp_c}h_1 + L_{c3}\dfrac{d\bar{\rho}_3}{dp_C}h_2\right) & A_c\left((\rho h)_{lg} - \bar{\rho}_3 h_2\right) & 0 \\ 0 & 0 & L_c \end{bmatrix}$$

and the condenser vector $\mathbf{f}_{c,R6}$

$$\mathbf{f}_{c,R6} = \begin{bmatrix} \dot{m}_{ci} - \dot{m}_{co} \\ -\dot{Q}_{cr2} + \dot{m}_{ci}h_1 - \dot{m}_{co}h_2 \\ \dfrac{\dot{Q}_{cr1-3} - \dot{Q}_{ca1-3}}{\left(c_p m/L_c\right)_{cw}} \end{bmatrix}$$

Reduced evaporator state vector now has the following form:

$$\mathbf{x}_{e,R6} = [p_c \quad L_{c2} \quad T_{cw}]^T$$

Reduced R6 evaporator matrix $\mathbf{A}_{e,R6}$ now has the following form:

$$\mathbf{A}_{e,R6} = \begin{bmatrix} A_e L_{e3}\left(\frac{d(\bar{\rho}_{e3}\bar{h}_{e3})}{dp_e} - \frac{d\bar{\rho}_{e3}}{dp_e}h_{e2}\right) & A_e\bar{\rho}_{e3}(h_{e2}-\bar{h}_{e3}) & 0 \\ A_e\left(L_{e2}\frac{d\rho_{elg}}{dp_e} + L_{e3}\frac{d\bar{\rho}_{e3}}{dp_e}\right) & A_e\left(\rho_{elg}-\bar{\rho}_3\right) & 0 \\ A_e\left(L_{e2}\left(\frac{d(\rho h)_{elg}}{dp_e} - 1\right) + L_{e3}\frac{d\bar{\rho}_3}{dp_3}h_{e3}\right) & A_e((\rho h)_{elg} - \bar{\rho}_3 h_{e2}) & 0 \\ 0 & 0 & L_e \end{bmatrix}$$

and the condenser vector $\mathbf{f}_{e,R6}$

$$\mathbf{f}_{e,R6} = \begin{bmatrix} \dot{m}_{ei} - \dot{m}_{eo} \\ \dot{Q}_{er2} + \dot{m}_{ei}h_{ei} - \dot{m}_{eo}h_{e1} \\ \frac{\dot{Q}_{ea} - \dot{Q}_{er2-3}}{\left(c_p m/L_e\right)_{ew}} \end{bmatrix}$$